A Comparison of Tropical Cyclone Projections in a High-resolution Global Climate Model and from Downscaling by Statistical and Statistical-deterministic Methods

Renzhi Jing,[a] Ning Lin,[a] Kerry Emanuel,[b] Gabriel Vecchi,[c] Thomas R. Knutson[d]

[a]*Department of Civil and Environmental Engineering, Princeton University*

[b]*Department of Earth, Atmospheric and Planetary Sciences, MIT*
[c]*Department of Geosciences, Princeton University*

[d]*Geophysical Fluid Dynamics Lab /NOAA*

[*]Corresponding: nlin@princton.edu

Corresponding author: Ning Lin, nlin@princeton.edu

ABSTRACT

In this study, we investigate the response of tropical cyclones (TCs) to climate change by using the Princeton environment-dependent probabilistic tropical cyclone (PepC) model and a statistical-deterministic method to downscale TCs using environmental conditions obtained from the Geophysical Fluid Dynamics Laboratory (GFDL) High-resolution Forecast-oriented Low Ocean Resolution (HiFLOR) model, under the Representative Concentration Pathway 4.5 (RCP4.5) emissions scenario for the North Atlantic basin. The downscaled TCs for the historical climate (1986-2005) are compared with those in the mid- (2016-35) and late-twenty-first century (2081-2100). The downscaled TCs are also compared with TCs explicitly simulated in HiFLOR. We show that while significantly more storms are detected in HiFLOR towards the end of the twenty-first century, the statistical-deterministic model projects a moderate increase in TC frequency, and PepC projects almost no increase in TC frequency. The changes in storm frequency in all three datasets are not significant in the mid-twenty-first century. All three project that storms will become more intense and the fraction of major hurricanes and Category 5 storms will significantly increase in the future climates. However, HiFLOR projects the largest increase in intensity while PepC projects the least. The results indicate that HiFLOR's TC projection is more sensitive to climate change effects and statistical models are less sensitive. Nevertheless, in all three datasets, storm intensification and frequency increase lead to relatively small changes in TC threat as measured by the return level of landfall intensity.

SIGNIFICANCE STATEMENT

The study provides the first comparison among TC climatology projections based on statistical, statistical-deterministic, and dynamic models driven by the same environmental

conditions. Under the projected climate for the RCP4.5 emissions scenario for North Atlantic, all three models project TC intensity to significantly increase, with the dynamic model HiFLOR projecting the largest increase in intensity. While HiFLOR projects a significant increase in TC frequency towards the end of the twenty-first century, the statistical-deterministic model projects a moderate increase in TC frequency, and the statistical model projects almost no increase in TC frequency. In all three datasets, storm intensification and frequency increase lead to relatively small changes in TC threat as measured by the return level of landfall intensity.

1. Introduction

Tropical cyclones (TCs) are among the most destructive natural hazards on the earth, and they have caused great economical and societal losses. Studies have shown that TCs may induce more damage under the impact of anthropogenic global warming (e.g., Mendelsohn et al., 2012). Though many studies have investigated how TCs will change in a changing climate, great uncertainties exist. The vast majority of published studies have suggested a decline in the global frequency of TCs with warming (e.g., Intergovernmental Panel on Climate Change (IPCC) 2013; Knutson et al. 2010; Walsh et al. 2016; Knutson et al. 2020), but a few others suggest an increase in TC frequency (Emanuel 2013; Bhatia et al. 2018; Fedorov et al. 2018, Vecchi et al. 2019). In a recent assessment (Knutson et al. 2020) most of the assessment's authors conclude that there is a low-to-medium confidence in a future global reduction of TC frequency, although there is considerable divergence of opinion among the author team of the assessment. Also, Knutson et al. (2020) find that there is less agreement among modeling studies on the projected sign of change in Atlantic basin frequency compared to the case for the global projections, although a clear majority of studies project a

63 decrease for the Atlantic basin. Contrary to the divergent projections in TC frequency, a
64 consensus has emerged about increased TC intensity as well as increased TC-induced rainfall
65 rates (Knutson et al. 2020; Knutson et al. 2013; Scoccimarro et al. 2014; Villarini and
66 Vecchi, 2012; Liu et al. 2019; Stansfield et al. 2020). Other storm-related hazards are also
67 shown to become exacerbated under climate change. For example, Marsooli et al. (2019)
68 suggest that hurricane flood hazards along the US Atlantic and Gulf coasts are likely to
69 significantly increase, due to storm changes as well as sea level rise. However, while there is
70 high confidence that sea level rise will add to storm inundation levels, the extent to which TC
71 intensity, rainfall, and storm-induced surge will increase remains quite uncertain (e.g.,
72 Knutson et al. 2020, Emanuel 2017, Marsooli et al. 2019; Garner et al. 2017). Improved
73 assessment of climate change effects on TC and TC-related hazards continues to be of great
74 importance for both scientific understanding and climate adaptation practice.

75 Three main modeling approaches are used to investigate the response of TC climatology
76 to climate change: general circulation models (GCMs), dynamic downscaling, and synthetic
77 downscaling. The previous generation of global climate models is widely used for global
78 projections; however, these models cannot directly simulate intense TCs due to their
79 relatively low resolution (Davis 2018). The dynamic downscaling techniques that are usually
80 paired with these low-resolution GCMs are alternative approaches to better resolve TCs.
81 Pioneered by Knutson et al. (1998) and Knutson and Tuleya (2004), dynamic downscaling
82 resolves the TC structure with an embedded higher-resolution regional model, which inherits
83 the environmental conditions from GCMs (Knutson et al. 2013; 2015). Although effective in
84 resolving individual storms, dynamic downscaling methods are still computationally
85 expensive and thus not ideal for TC risk assessment studies, where large numbers of storms

86 (~10^4) are often needed to evaluate the risk posed to a specific region (e.g., Lin and Emanuel
87 2016).

88 Recently a few GCMs have been able to explicitly simulate intense TCs. This eliminates
89 the need for a separate dynamical downscaling step for the GCMs in climate change
90 experiments (Wehner et al .2014). These GCMs have grid spacings of 28 km or finer and can
91 explicitly represent Category 4 and 5 TCs [e.g., Centro Euro-Mediterraneo sui Cambiamenti
92 Climatici Climate Model (CMCC-CM2-VHR) developed by Scoccimarro et al. (2017),
93 Community Earth System Model (CESM) developed by Small et al. (2014)]. In particular,
94 the Geophysical Fluid Dynamics Laboratory (GFDL) High-resolution Forecast-oriented Low
95 Ocean Resolution (HiFLOR), which is a high-resolution atmospheric/land model
96 (0.25°×0.25°) coupled with a low-resolution oceanic/sea ice model (1°×1°, Murakami et al.
97 2015), can reproduce many features of TC climatology, including spatial distribution and
98 intensity distribution, with good fidelity compared to observations (Murakami et al. 2015;
99 Zhang et al. 2016). Previous studies using HiFLOR projections identify an increase in the TC
100 intensification rate and a higher chance of TC rapid intensification (RI) by the end of the
101 twenty-first century (Bhatia et al. 2018), as well as an increase in global TC frequency and in
102 the frequency of the most intense (Cat 3-4-5 and Cat. 4-5) TCs in response to increasing
103 greenhouse gases (Bhatia et al. 2018; Vecchi et al. 2019). Not all models with grid spacing
104 of 28 km or finer are able to simulate very intense (Category 4 or 5) TCs (e.g., Yamada et al.
105 2017, Manganello et al. 2014, Knutson et al. 2008), as this capability appears to depend on
106 both model resolution and details of model physics.

107 Synthetic downscaling methods, which are now commonly used for climate-TC risk
108 studies, generate large numbers of synthetic TCs at the basin scale based on comprehensive
109 climate conditions from reanalysis data or low-resolution GCM simulations. The pioneer of

this family of methods is the statistical-deterministic method developed by Emanuel et al. (2008). This method applies a random seeding technique to initiate the storm, a beta and advection model based on synthetic local winds to propagate the storm, and a deterministic intensity model (CHIPS, Coupled Hurricane Intensity Prediction System; Emanuel et al., 2004) to estimate the storm intensity based on the storm environment along the track. This method has been applied to study TC properties under various climate conditions. In particular, Emanuel et al. (2013) apply the method to downscale six CMIP5 climate projections and project an increase in TC frequency during the twenty-first century. The method has also been widely applied to assess TC wind (Yeo et al., 2014), rainfall (Emanuel, 2017), and storm surge (Marsooli et al., 2019) hazards as well as TC economic losses (Mendelsohn et al., 2012), under current and future projected climate conditions.

Similar to Emanuel et al. (2008), the model developed by Lee et al. (2018) can also generate synthetic TCs for given climate conditions, but it is purely statistical. This model has a genesis component based on Poisson regression (Tippett et al. 2011). Its track component is based on a revised beta and advection model with the beta drift term dependent on the storm location, and its intensity component is based on multiple linear regression on key environmental parameters plus an autoregressive stochastic error term (Lee et al., 2015, 2016). Diverging TC frequency trends are projected using this method to downscale five CMIP5 climate projections, where the storm frequency will increase or decrease depending on the selection of the moisture variable (relative humidity or saturation deficit) in its genesis component (Lee et al. 2020).

Recently, a new probabilistic TC model, the Princeton environment-dependent probabilistic tropical Cyclone model (PepC), has been developed by Jing and Lin (2020). Aimed to improve over Lee et al. (2018), PepC performs the Poisson regression on

environment-clustering grids (rather than regular grids) to better capture the spatial-temporal variation of the storm genesis. PepC applies an analog-wind track model where storm tracks are determined based on similar historical track patterns in addition to local in situ wind, which allows the model to better capture intrinsic features such as recurving storm tracks at high latitudes. It models the evolution of a storm's intensity as a Markov process to better capture the nonlinear/nonhomogeneous response of TC intensification to the environmental change along the storm track. As a result, although most statistical TC intensity models have only limited capacity to simulate extreme TCs, PepC can simulate a realistic fraction of RI storms due to its "lock-in" mechanism, which supports continuous rapid intensification once the storm enters the extreme state of intensification when the environment is favorable. The capacity to simulate extreme TCs is essential, especially for climate change studies where a number of modeling studies suggest that higher intensity TCs are more likely to increase in frequency than lower intensity TCs under global warming (Knutson et al. 2020).

While widely used in climatology modeling and risk assessment, the synthetic downscaling methods described above have not been compared in terms of their TC projections under climate change scenarios. These synthetic downscaling methods are fully (Lee et al. 2018, Jing and Lin 2020) or partially (Emanuel et al. 2008) statistical. It is important to compare their TC climatology projections with those based on full dynamic modeling (Emanuel et al. 2010). Also, most existing TC projections were driven by varying environmental conditions (generated from different climate models and/or for difference emissions scenarios, Knutson et al. 2020); comparisons among TC projections that are driven by the same environmental condition are limited. By holding the environmental condition fixed across the methods, any differences in response are due to factors other than differences in the large-scale TC environment as simulated by climate models. In addition to their

158 practical importance, such comparisons may also contribute to our understanding of how TCs
159 will respond to climate change.

160 In this study, we apply both the PepC of Jing and Lin (2020) and the statistical-
161 deterministic model of Emanuel et al. (2008) to generate large samples of synthetic TCs
162 under HiFLOR projected climates for the Atlantic Basin, where the PepC has been tested
163 against observations (Jing and Lin 2020). The synthetic storms downscaled from the HiFLOR
164 climate projections are compared with storms generated directly in HiFLOR. We use three
165 HiFLOR experiments to represent the historical ("control," 1986–2005) and future ("early,"
166 2016–35 and "late," 2081–2100) climates under the Representative Concentration Pathway
167 4.5 (RCP4.5) scenario; these are the same experiments explored in van der Wiel et al. (2017)
168 and Bhatia et al. (2018). In addition to examining the discrepancies in the modeling
169 approaches and results, we investigate simulated TC characteristics under the historical and
170 future climates to study the climate change effects. The climatology characteristics we focus
171 on include storm basin-wide annual frequency, track density, and lifetime maximum
172 intensity, as well as landfall frequency, intensity, and return periods. We further discuss the
173 modeling results in comparison with previous TC projections.

174 This paper is organized as follows. After this introduction, Section 2 describes the high-
175 resolution GCM applied, HiFLOR; the two downscaling techniques, Emanuel et. al (2008)
176 and Jing and Lin (2020); and the downscaling experiments. Section 3 presents simulated
177 results under current and future climates. Section 4 discusses TC frequency trend and
178 possible attributions. Section 5 concludes the study.

179

180 2. Data, Models, and Downscaling Approaches

In this section, we first describe the HiFLOR model and the three HiFLOR experiments used in this study. Next, we briefly describe the two downscaling approaches, Emanuel et al. (2008) and Jing and Lin (2020). The calibration methods associated with each downscaling approach are also explained.

a. HiFLOR model and experiments

In this study, we use three 70-year HiFLOR "time slice" climate experiments (i.e., repeating climatological forcing for each simulation year, as introduced in van der Wiel et al. 2017) to represent the effects of climate change. The control experiment represents the historical climate during the period of 1986–2005, while two future climate experiments, the "early" and "late" experiments, project the climate during 2016–35 and 2081–2100, respectively. The experiments are set up with sea surface temperature (SST) relaxed to climatological SST values. The prescribed SST target in the control experiment is set as the monthly varying climatology from the Met Office Hadley Centre Sea Ice and SST dataset (HadISST1.1; Rayner et al. 2003) over 1986–2005, while the "early" and "late" experiments used the same climatological values of SSTs from the control experiment plus the projected changes in 2016-35 and 2081-2100, respectively, derived from a multi-model mean of 17 CMIP5 models, based on the RCP 4.5 pathway (Van Vuuren et al. 2011). The experiments cannot capture the response of TC activity to SST changes in the interannual or decadal scales. However, it is hypothesized that those variations are smaller than the response of TC activity to climatological changes in SST – a hypothesis that is supported by fully coupled and nudged-SST experiments (Vecchi et al. 2019).

TCs in HiFLOR are tracked based on warm-core temperature, sea level pressure, and 10-m wind. This tracker, developed by Harris et al. (2016), is applied to 6-hourly instantaneous output from the model using the parameter values of Zhang et al. (2016), Murakami et al.

205 (2015), Bhatia et al. (2018), and Vecchi et al. (2019). Specifically, the tracker follows local
206 sea level pressure minima, and TCs are identified using a wind speed threshold (17.5 m/s)
207 and a warm core threshold of 2 K within 1° of the storm center. TCs are required to have a
208 72-h total detection lifetime with at least 48 cumulative hours with a warm core and 36
209 consecutive hours with peak winds exceeding 17.5 m/s, and location of TC genesis should be
210 equatorward of 40°. HiFLOR TCs are shown to closely resemble the observational hurricane
211 datasets, including the International Best Track Archive for Climate Stewardship (IBTrACS,
212 Knapp et al. 2010) and the advanced Dvorak technique-Hurricane Satellite-B1 (ADT-
213 HURSAT, Kossin et al. 2013), for the North Atlantic Basin, which has the most reliable data
214 quality given its superior observational network (Kossin et al., 2013; Bhatia et al., 2019).
215 HiFLOR has been shown to produce skillful seasonal predictions of regional TC activity and
216 Cat. 4-5 frequency (Murakami et al. 2016). Besides TC characteristics, HiFLOR also outputs
217 major environmental parameters including daily temperature, moisture, pressure, wind, etc.,
218 which are used to drive the synthetic downscaling.

219 *b. The statistical-deterministic method of Emanuel et al. (2008)*

220 This subsection briefly describes the statistical-deterministic downscaling method, and we
221 refer readers to Emanuel et al. (2008) for more details of the model. First, storms are
222 initialized with random seeding in space and time, and each seed is randomly assigned an
223 initial wind speed that is less than 25 kt. The random seeding rate is tapered down near the
224 equator, in proportion to the low-level absolute vorticity, to prevent storm formation close to
225 the equator. Next, storm movements are determined by a beta and advection model driven by
226 large-scale background winds synthetically generated from a global model projection or
227 reanalysis dataset and beta drift approximated as a function of latitude (in the updated version
228 of the model used in this study). Then, the wind field of each storm is predicted using an

229 atmosphere-ocean coupled model, CHIPS, which has very high radial resolution of the
230 critical inner-core region and can resolve high-intensity storms. This simplified deterministic
231 intensity model is computationally efficient, making it possible to generate very large
232 numbers of TCs at a low computational cost. It is noted that the random seeding technique in
233 Emanuel et al. (2008) does not produce an absolute rate of genesis per unit time per unit area;
234 therefore, the genesis rate is often calibrated by setting the annual global or basin-wide
235 number of genesis events under the control climate to the observed genesis rate in the
236 historical period. The calibration constant obtained from the control climate is then used as a
237 multiplicative factor for the future climate experiments. This statistical-deterministic
238 downscaling method is shown to generate synthetic storms that are in statistical agreement
239 with observations (Emanuel et al. 2006). There are in total 1151, 1095 and 1049 storms
240 generated from the statistical-deterministic under the control, "early" and "late" experiments
241 for the North Atlantic basin in this study.

242

243 *c. PepC of Jing and Lin (2020)*

244 The PepC model developed in Jing and Lin (2020) is also used to perform downscaling of
245 HiFLOR under each climate condition. PepC consists of a clustering-based genesis model, an
246 analog-wind track model, and a Markov-based intensity model. The genesis model seeds
247 weak vortices in the basin based on Poisson regression on the environmental parameters
248 including Potential Intensity (PI, derived following Emanuel (1995) and Bister and Emanuel
249 (1998; 2002)), deep layer vertical wind shear (SHR), low-level relative vorticity (VO), and
250 saturation deficit (derived following Emanuel et al. 2008), over clustering grids that are
251 determined by the similarity of these local environmental conditions. Compared to Emanuel

et al. (2008), where the genesis seeding does not evolve with climate change[1], the genesis distribution in Jing and Lin (2020) is highly dependent on climate variables. We use saturation deficit as the humidity predictor in this study on climate change impact given that theoretically saturation deficit better reflects the increase in the thermodynamic inhibition of TC formation in a warming climate (Emanuel et al. 2008), although Jing and Lin (2020) show that using relative humidity fits better statistically with the observations under the current climate. After initialization, the seeds are passed to an analog-wind track model, in which a storm's movement is determined by both analog factors (from historical track patterns) and local in-situ winds. The wind predictors are similar to those in the beta and advection model in Emanuel et al. (2008) and are derived from large-scale global model or reanalysis wind fields.

The storm's intensity is determined by the Markov environment-dependent hurricane intensity model (MeHiM), which simulates TC intensity evolution over the ocean as a Markov process (Jing and Lin, 2019). MeHiM considers three unobserved (hidden) discrete states of intensification and associates each state with a probability distribution of intensity change. The three unobserved discrete states, the "static," "moderate," and "extreme" states, represent the storm's slow, normal, and rapid intensity changes, respectively. The storm's transit from one state to another is described as a Markov chain. Both the intensity change

[1] Aside from minor changes in seeding rate near the equator, owing to possible changes in the absolute vorticity of the low-level flow there.

and state transit components of the MeHiM are dependent on environmental variables, including PI, SHR, relative humidity (RH), and an ocean feedback parameter (incorporating vertical profiles of oceanic temperature and salinity; derived following Schade and Emanuel 1999), in addition to the storm's last step intensity change and current intensity. Jing and Lin (2019) show that it is important to include in MeHiM an ocean feedback parameter to represent the ocean's cooling effect, which is often omitted in other statistical downscaling methods (Murakami et al. 2012; Korty et al. 2017). The ocean feedback parameter, included in the MeHiM used in this study, is also estimated from HiFLOR. A simple land model (similar to DeMaria and Kaplan, 1995; see more details in Jing and Lin 2019) is added to estimate intensity decay as a function of time when the storm moves over land.

The original PepC model in Jing and Lin (2020) is developed based on observational reanalysis data, and the simulated results compare well with observations (Jing and Lin 2020). When applied to downscale climate model projections, however, PepC may produce biased results due to possible biases in the climate model projections. To focus on the climate change effects based on the HiFLOR simulations in this study, therefore, we "calibrate" PepC by adjusting each of its model components to capture the HiFLOR climate-TC relationships in the control experiment. That is, we redevelop each of the genesis, track, and intensity components of PepC based on HiFLOR simulated storms and the environment in the control experiment. Then we apply the fitted model to generate synthetic storms for each of HiFLOR control and future climate experiments. There are in total 36232, 39997 and 41131 storms generated from PepC under the control, "early" and "late" experiments for the North Atlantic basin in this study.

3. Results

In this section, we investigate the response of simulated TCs to climate change in each dataset moving from control to "early" and "late" experiments. The HiFLOR model-generated TCs are detected by a strict detection algorithm, as mentioned above. To be consistent with HiFLOR, we filter the synthetic TCs generated by downscaling techniques in Emanuel et al. (2008) and PepC to include only storms that last at least 72 hours and have at least 36 consecutive hours of winds greater than 34 kt. To be clear, in the following sections, we use "HiFLOR" to specifically refer to the TCs that are explicitly simulated in HiFLOR experiments. We denote the TC dataset downscaled from HiFLOR experiments with the Emanuel et. al (2008) approach as "KE08" and the TC dataset downscaled with the Jing and Lin (2020) approach as "PepC". The observational TC data in the period of 1986-2005, taken from the IBTrACS WMO archive (Knapp et al. 2010), are used as a reference. The data include 6-hourly latitude and longitude positions as well as 10-minute maximum sustained wind speeds at 10 m above the sea surface for each storm. The observational dataset is denoted as "IBTrACS". We compare "KE08" and "PepC" to "HiFLOR" to discuss the TC differences between synthetic downscaling and original climate model projections under the same climate environments (HiFLOR control and climate projections under RCP4.5). In addition, we present "IBTrACS" as a reference to possibly detect the effects of biases in the HiFLOR climate estimation.

a. Annual Frequency and Genesis Distribution

We first examine the annual frequency of Atlantic storms from HiFLOR, KE08, and PepC. There are on average 9.1 storms/year in HiFLOR under the control experiment, which is comparable to 10.15 storms/year in IBTrACS. There are 11.8 and 7.25 storms per year in KE08 and PepC under the control experiment, respectively. The original genesis frequency in

PepC (9.3) is close to that in HiFLOR, as the genesis component in PepC is developed based on HiFLOR genesis under the control experiment. However, only 78% of the storms develop to meet the storm selection criteria described above. It is also noted that the storm frequency in KE08 is larger than the other datasets. The genesis in KE08 is generated through random seeding, which is calibrated with the observed global frequency. Here, to focus on the climate change effects, we further calibrate TC frequency in PepC and KE08 to be consistent with HiFLOR in the control experiment for the North Atlantic basin. Specifically, we apply a multiplicative factor of 0.77 to KE08 and of 1.3 to PepC, for both the control experiment and future climate projections. The resulting estimations of annual frequency of total storms and major hurricanes (discussed later) for the three models appear in Fig. 1.

To determine whether the change of storm frequency from the control to climate change scenarios is statistically significant, we perform hypothesis testing of equal frequency for each dataset. The two-sample, unpaired t-test (Wilks 2011) is computed for HiFLOR and KE08, and a p-value of 0.05 is set as the threshold for statistical significance. To adjust for multiple comparisons (we have 100 realizations of PepC downscaling, and each realization is compared with HiFLOR for the hypothesis test), the Benjamini and Yekutieli (2001, 2005) procedure of controlling the false discovery rate (FDR) of a family of hypothesis tests is performed for PepC, with the same statistical significance threshold of p-value of 0.05. When the p-value is less than the threshold of 0.05, we reject the null hypothesis and consider the change in TC frequency statistically significant. Statistically significant change in TC frequency indicates that the change is very likely not induced by randomness. As shown in Table 1, HiFLOR has a significant increase of storm frequency in the “late” experiment compared to the control experiment (+22.4%), while the increase in the “early” experiment (+8.2%) is not statistically significant. Similarly but to a lesser extent, KE08 has a significant

increase in the storm frequency in the “late” experiment compared to the control experiment (+8.5%); however, KE08 has a nonsignificant decrease in the “early” experiment (-4.4%). PepC has a nonsignificant decrease (-0.6%) in the storm frequency in the “early” experiment and a nonsignificant increase (+2.2%) in the “late” experiment.

In addition to the annual frequency, the spatial distributions of TC genesis in the datasets under the control experiment are shown in Figure 2. Compared to HiFLOR, KE08 shows a similar genesis pattern; however, the maximum in the main development region (MDR, 10N-20N, 80W-20W) is slightly shifted to the east, and slightly more storms are generated in the Gulf of Mexico and Caribbean regions. PepC captures genesis pattern in HiFLOR, though the storms are much less concentrated in the MDR and spread more to the middle of the Atlantic. The genesis scheme for KE08 and PepC are quite different. In KE08, as the storms are randomly seeded everywhere (with the exception of tapering near the equator), the spatial pattern of genesis indicates that the storm survival rate in the MDR is much higher than in any other regions. However, in PepC where storms are initiated based on local climate conditions, the genesis spatial distribution is determined by both the initial distribution and survival rate.

Historically, the majority of storms form in the MDR, but secondary maxima of activity are seen off the U.S. southeast coast and in the Gulf of Mexico (Fig. 2a). The control simulations capture the maximum in the MDR with the hotspot shifted to the west of the MDR. However, the simulations do not produce much concentrated activity along the U.S. coast or in the Gulf of Mexico, as shown in IBTrACS, probably due to the bias in the simulated climate environment. The statistical significance of these differences cannot be easily tested given the limited sample size in IBTrACS at the local scale. It is worth mentioning that the spatial distribution of genesis in KE08 is similar to that in Emanuel et. al

365 (2008) when the synthetic storms are downscaled from the reanalysis data, indicating that the
366 random seeding technique is relatively stable and less sensitive to changes and potential
367 biases in the climate estimation. No significant changes in TC genesis locations are identified
368 in the future climate projections (figures not shown).

369 *b. Track Density and Landfall Frequency*

370 Figure 3 compares the track density of the datasets for the control experiment. TC track
371 density is calculated by counting the number of times per year that TC tracks pass each 5°×5°
372 grid cell. The track density plot of IBTrACS is also shown as a reference. Although the track
373 density is highly affected by the genesis distribution (Fig. 2), the track density in PepC
374 compares closely to that in HiFLOR, as PepC tracks depend on HiFLOR's track pattern and
375 environmental wind. Both have a single maximum in the western North Atlantic around
376 25^{o}N, 70^{o}W; both show the typical recurving pattern in tracks, though storms in PepC recurve
377 slightly earlier than those in HiFLOR. Also, the track distributions in both HiFLOR and PepC
378 have a tongue extending towards the Gulf of Mexico, although the tongue in HiFLOR is
379 slightly larger than that in PepC. The track density of KE08 is quite different from those of
380 HiFLOR and PepC, although the genesis distribution in KE08 is similar to that in HiFLOR
381 (Fig. 2). There are many more storms in KE08 that travel towards Gulf of Mexico, while
382 much less are recurving to high latitudes, which results in a stronger maximum appearing in
383 the Gulf of Mexico compared to HiFLOR and PepC. This difference is likely due to the fact
384 that the track component in Emanuel et al. (2008) depends mainly on the environmental wind
385 that is synthetically generated based on the monthly wind climatology from HiFLOR, and the
386 effect of beta drift is approximated as a simple function of latitude. Compared to the
387 IBTrACS, HiFLOR and PepC's maxima in western North Atlantic are large and shifted away
388 from the US southeast coast, while for KE08 the track density is more highly concentrated

389 along a path between the MDR and the Gulf of Mexico; these modeling errors are induced by
390 a mixture of uncertainties in the TC models and HiFLOR climate estimation. It should also be
391 noted that the synthetic downscaling simulations do not include hybrid storms, which are
392 present in the observations and possibly also in the HiFLOR simulations.

393 We further examine regional annual landfall frequency at coastal locations along the
394 North Atlantic coastline. To help indicate locations, a total of 186 mileposts (MPs) is defined,
395 following Vickery et al. (2000) and Jing and Lin (2020), to cover the coastline with 100-km
396 spacing along the Mexican coastline and 50-km spacing along the U.S. coastline, as shown in
397 Fig. 4. Here, landfall is defined as the passing of a storm within 100 km of each milepost. As
398 shown in Fig. 5(a) for the control experiment, the simulated annual landfall frequencies of
399 KE08 and PepC are compared with those of HiFLOR for the mileposts. (Given its limited
400 sample size at the local scale, IBTrACS is not used for comparison here.) In general, KE08
401 has a correlation coefficient of 0.55 with HiFLOR, compared with 0.80 of PepC with
402 HiFLOR. PepC is in good agreement with HiFLOR in terms of variations for almost all
403 mileposts. However, it shows a slight overestimation near MP 40-50 but a negative bias to
404 the north of MP 50, likely due to the fact that storms in PepC tend to recurve earlier (Fig. 3).
405 KE08 shows larger variations. In all regions south of MP 100 (west of Florida), KE08 has
406 much higher landfall frequency than HiFLOR and PepC, while in regions north of MP 100,
407 the landfall frequency of KE08 drops dramatically and becomes much lower than that of
408 HiFLOR, close to PepC to the north of MP 120. These results are also consistent with the
409 track density plot as shown in Fig. 3, where most storms in KE08 travel to the Gulf of
410 Mexico.

411 Fig. 5(b-d) compares the TC annual landfall frequency at the 186 mileposts in the control
412 and climate change experiments. We find that the climate change effect on landfall frequency

is relatively small, compared to the variation of the predictions among the models. HiFLOR is the most sensitive to climate change, with some increases shown in the "early" experiment for the south of MP100 (south of Florida) and in the "late" experiment for the north of MP100, while PepC shows the least sensitivity with almost no change except for a slight increase in the "late" experiment for MP 80-110, which represents the Florida area. It is interesting to find that even though a significant increase exists in the frequency of total TCs in HiFLOR and KE08 (+22.4% and +8.5%; Table 1), changes in their landfall frequency appear to be smaller.

c. LMI, Rapid Intensification rate and Landfall Intensity

Next, we examine the intensity properties of the simulated storms. Fig. 6 (a) shows the probability density functions (PDFs) of TC lifetime maximum intensity (LMI) for storms in HiFLOR, KE08, and PepC in the control experiment. The LMI distribution of HiFLOR follows a bimodal distribution, with the first peak located at about 75 kt. In HiFLOR, about 35% TCs reach major hurricane intensities, and around 1% grow to Category 5 (LMI > 136 kt) storm. Around 45% of HiFLOR storms undergo RI. Compared to HiFLOR, KE08 simulates much weaker storms with the peak appearing at around 70 kt. Only 31% of storms undergo RI during their lifecycle, and only 22% of storms reach major hurricane intensity. However, 1% become the most intense Category 5 storms, which is similar to HiFLOR. PepC stands in the middle between HiFLOR and KE08. It also follows a bimodal distribution, with the first peak, however, close to that of KE08. Generally speaking, there are more storms with moderate LMI in PepC than in KE08 and HiFLOR. Around 28% of PepC storms reach major hurricane intensity, 33% undergo RI, and 1% grow to Category 5.

The LMI of IBTrACS is also shown in Fig. 6 (a) as a reference. Historically, 30% of storms reach major hurricane intensity, about 4% grow to Category 5, and around 45%

437 undergo RI. Compared to observations, there are fewer weak and very strong storms in
438 HiFLOR (and also in PepC), and the LMIs are more concentrated in a narrower range. This
439 inconsistency could be partially induced by the detection algorithm, as the warm-core
440 requirements and other components of the detecting procedure in HiFLOR may have lowered
441 the number of weak TCs, which shifts the first peak of the LMI distribution to a higher value.
442 It is noted that these results are very similar to findings in Bhatia et al. (2018), in which a
443 similar HiFLOR simulated storm dataset is used. All three simulations underestimate the tail
444 of LMI as shown for IBTrACS.

445 We then examine the PDFs of TC LMI in HiFLOR, KE08 and PepC in the "early" and
446 "late" experiments. In all three datasets, the entire LMI distributions shift to higher intensity
447 values in climate change experiments. However, HiFLOR has the largest change while PepC
448 has the least change (Fig. 6b-6d). As shown in Fig. 1 and Table 1, HiFLOR has significantly
449 more major hurricanes in the "early" (+24%) and "late" (+60.4%) than in the control
450 experiment. HiFLOR has particularly large increases in Category 4 (+103.2%) and Category
451 5 (+540%) in the "late" experiment. These results are consistent with the analysis in Bhatia et
452 al. (2018) for the North Atlantic basin. To a lesser extent, KE08 shows significant increases
453 in the major hurricanes (+37.8%) and Category 5 storms (+250%) in the "late" experiment.
454 Similar to HiFLOR, PepC projects increases in major hurricanes (+17.1%), Category 4
455 storms (+29.4%), and Category 5 (+53.6%) storms in the "late" experiment; the changes are
456 much smaller but still significant.

457 As most Category 4 and 5 storms undergo RI during their lifecycles, we further
458 investigate the change in RI storms. HiFLOR has a significant increase of the RI storms in
459 both the "early" (+39.6%) and "late" (+76%) experiments. KE08 and PepC have significant
460 increases of the RI storms in only the "late" experiment (+20.5% and +10.8%, respectively).

461 Related to the differences in the RI rate among the three datasets, there are around 24%, 11%,
462 and 14% Category 4 storms and 4%, 5%, and 1% Category 5 storms projected in HiFLOR,
463 KE08, and PepC, respectively, leading to very different tails (LMI >125 kt) of the LMI
464 distributions among the three datasets in the "late" experiment although these tails are very
465 similar in the control experiment (Fig. 6).

466 Next, we investigate the probability distribution of the landfall intensity for the North
467 Atlantic coastline and its divisions of the U.S. into the Northeast, Southeast, and Gulf of
468 Mexico regions (Fig. 7, with the definition of regions denoted in Fig. 4). In this case, TC
469 landfall is defined as crossing the coastline for each region. In the control experiment, in
470 contrast to the LMI case, where PepC stands in the middle of HiFLOR and KE08, PepC has a
471 higher portion of intense landfalling hurricanes, especially when the landfall intensity is
472 greater than 70 kt. Landfalling TCs in HiFLOR are weaker than those in PepC, followed by
473 those in KE08, which have the lowest landfall intensities, with the peak of the distribution
474 located around 35 kt (although IBTrACS has an even lower peak around 25 kt). The
475 distributions of landfall intensity in the three subregions have similar patterns to those for the
476 entire US coastline, except that in the North-East U.S., the distribution of KE08 is more
477 significantly left-shifted than in either PepC and HiFLOR. This discrepancy can be explained
478 by the difference in the TC tracks, as shown in Fig. 3. As most storms in KE08 travel to the
479 Gulf of Mexico, fewer storms grow, intensify, and eventually make landfall in the
480 northeastern region. Compared to IBTrACS, the simulations, especially HiFLOR and PepC,
481 have higher landfall intensity except at the very end of the tail, which is consistent with the
482 LMI properties shown above.

483 There is not much change in the landfall intensity when the climate moves from the
484 control experiment to the "early" and "late" experiments, as shown in Fig. 7. We identify

485 only slight shifts toward large-intensity values in the northeastern and southeastern U.S. in all
486 three datasets. However, all changes fail the Two-sample Kolmogorov-Smirnov test on
487 differences in distributions and are hence statistically negligible. Referring to Table 1 and
488 Fig. 6, storms are projected to become more intense overall, especially in HiFLOR, but this
489 intensification does not carry over to landfall at regional or basin scale in the three simulation
490 datasets.

491 *d. Return Period of Landfall Intensity*

492 Combining the landfall frequency and landfall intensity distribution, we compute return
493 periods for landfall intensities to describe potential TC threat along the U.S. coastline. The
494 return period for an intensity level is the inverse of the corresponding annual exceedance
495 probability, which describes the chance of one or more TCs making landfall with an intensity
496 greater than the intensity level in any given year (under a specific climate condition). The
497 annual exceedance probability is calculated as the product of landfall frequency and
498 exceedance probability of the landfall intensity. We show TC landfall intensity as a function
499 of return period for each of the segments of the U.S. coastline (illustrated in Fig. 4, where TC
500 landfall is defined as crossing the coastline for each region), for each model and climate
501 condition.

502 The return period curves of HiFLOR, PepC and KE08 are shown in Fig. 8. The return
503 period curves for IBTrACS are also shown in Fig. 8 as a reference. In the control experiment,
504 for the U.S. coastline, the return period curve in PepC is the lowest, KE08 is the highest, and
505 HiFLOR stands in the middle; IBTrACS is covered by the model spread. The return period
506 curves for the northeastern U.S. are more spread out, with KE08 the lowest, HiFLOR the
507 highest, and PepC in the middle and being closest to IBTrACS. The return period curves for
508 the Mexico are also spread out, and the KE08 distribution is much higher than HiFLOR and

PepC but happens to be the closest to IBTrACS. In the U.S. Southeast, the three datasets agree with each other and with IBTrACS, and the return period curves almost overlap. As the landfall intensity distributions for the three datasets are similar for Mexico (Fig. 7a), the much higher return period curve in KE08 is induced by its estimated much higher landfall frequency for this region (as indicated in Fig. 5a and Fig. 3). For the Northeast, the much lower return period curve in KE08 is induced by its estimated much lower landfall frequency (see Fig. 5a) and landfall intensity (Fig. 7a). The estimated lower frequency in PepC compared to HiFLOR for the Northeast (see Fig. 5a) also induces a lower return period curve for the region. The return periods for the U.S. coastline seem to be largely determined by those for the Mexico and southeastern U.S..

Next, we compute return period curves for HiFLOR, KE08 and PepC in the "early" and "late" experiments to investigate their responses to climate change. Overall, there is little systematic change of the landfall intensity return period under future climates compared to the current climate, especially at the basin scale. The relatively unchanged return periods result from the nonsignificant change in landfall intensity (Fig. 7) and in landfall frequency for most cases. The change in landfall frequency is statistically significant only in HiFLOR's "late" experiment for the northeastern U.S., based on the two-sample, unpaired t-test (Wilks 2011). Thus, for HiFLOR (Fig. 8b), there is a moderate increase in the return level for the northeastern U.S., due to the statistically significant increase in landfall frequency (see also Fig. 5b) and a nonsignificant increase in landfall intensity (Fig. 7b), and a slight decrease for Mexico in the future climate. As a result, there is little net change in the return level for the entire U.S. coastline. Nevertheless, the HiFLOR projection indicates that, although the northeastern region has the smallest TC threat, with the 100-year landfall intensity about 100 kt under the control climate, it is the region where the TC threat may grow the fastest as the

533 climate warms. The 100-year return level is projected to be as high as 110 kt in the "early"
534 experiment and 125 kt in the "late" experiment. In contrast, in Mexico the TC threat may
535 even slightly decrease under a warmer climate. For KE08, the return level increases only
536 slightly for the U.S. coastline, the southeastern U.S., and Mexico, with almost no change for
537 the northeastern U.S. (Fig. 8c). In contrast to HiFLOR and KE08, PepC has a slight increase
538 in landfall intensity level for the "early" experiment but almost no change for the "late"
539 experiment, compared to the control experiment (Fig. 8d). Overall, all three models predict
540 the climate change effect on the landfall intensity return level/TC threat to be quite small and
541 much smaller than the variation of the predictions among the models (Fig. 8a).

542

543 ## 4. Discussion

544 One main objective of this study is to evaluate a new statistical synthetic downscaling
545 approach to estimating how tropical cyclone activity will respond to climate change. Prior to
546 this study, statistical models (describing storm genesis, track, and intensity) are usually not
547 applied in TC climate change studies since most statistical models are climate-invariant. One
548 exception is Lee et al. (2020), who investigate TC activity by downscaling CMIP5 climate
549 models using the statistical model CHAZ (Lee et al. 2018). They show that the projected
550 future TC activity is very sensitive to the choice of humidity variable (saturation deficit or
551 relative humidity) used in the genesis component. This choice will lead to divergent
552 conclusions about annual TC frequency trends and thus large uncertainty in regional and
553 local storm hazard assessment. This finding reminds us that one must be cautious when using
554 statistical methods to project TC activity under future climate conditions. Here, for the first
555 time, we investigate statistical projections of future TC activity in comparison with dynamic
556 and statistical-deterministic projections, all for the same environmental condition changes.

Comparing storms generated and downscaled from HiFLOR projected climate (RCP4.5), we find that HiFLOR, KE08, and PepC show similarities in responding to climate change in that storms will become more intense. Significant increases in the frequency of major hurricanes and Category 5 hurricanes appear in all three datasets by the end of the twenty-first century, when the fractions of RI storms also increase significantly. For total storm frequency, HiFLOR suggests a large increase, KE08 suggests a moderate (but still significant) increase, and PepC suggests no significant change by the end of the twenty-first century. In general, the changes in PepC are usually smaller than those in HiFLOR and KE08, which means PepC is less sensitive to climate change effects. These results might indicate more generally that statistical methods are less sensitive than dynamic models to the changes in the climate environment that general circulation models project.

To further explore the causes of the uncertainties in the projections, we compare results in this study with those in the existing literature. The changes in the overall fraction of Cat 4-5 hurricanes in HiFLOR (+126%) and to a lesser extent in KE08 (+46%) and PepC (+45%) are significantly larger than the median projected global change of +13% in previous studies (Knutson et al. 2020), although the studies assessed in the Knutson et al. (2020) include a number of lower resolution models, where in some cases intense TC activity is inferred statistically rather than through direct simulation. Larger uncertainty exists in the projection of total storm frequency and of Cat 4-5 frequency. The Knutson et al. (2020) assessment suggests that the majority of dynamical modeling studies project a decline in the number of Atlantic TCs with global warming, and the model results are relatively split on whether Atlantic Cat-4-5 TC frequency will increase or decrease (with the caveat of the inclusion of statistically derived results from relatively low-resolution models). Analyzing eight CMIP5 climate model projections under the RCP 8.5 scenario, Tory et al. (2013) infer a mixture of

581 TC frequency increases and decreases for the Atlantic basin, based on an empirical TC
582 detection method. Their findings are more mixed than those of Knutson et al. (2013), who
583 find a clear preference for a projected overall decrease in Atlantic basin TC frequency
584 (significant for seven of ten individual CMIP3 models) along with a weak tendency (eight of
585 12 models) for an increase in the frequency of intense (Cat 4-5) TCs, using a variety of
586 CMIP3 and CMIP5 model scenarios as the boundary forcing. [Note that the range of
587 projections found by Knutson et al. (2013) and Troy et al. (2013) in downscaling different
588 CMIP3 models (e.g., as shown in Table 5 of Knutson et al. 2013) demonstrates that a wide
589 range of projections can be driven not only by different downscaling techniques, as illustrated
590 in the present study, but also by different climate models that supply information to the
591 downscaling framework.] In Knutson et al. (2015), which is based on downscaling TC cases
592 from the GFDL HiRAM global model under the RCP 4.5 emission scenario, only
593 inconclusive (non-significant) decreases in total TC frequency and non-significant increases
594 in Cat 4-5 frequency in the North Atlantic basin are projected (Table 3 of Knutson et al.
595 2015). Other recent studies suggest no change or even an increase in TC frequency under the
596 future climate. Applying a statistical downscaling scheme to seventeen CMIP5 models,
597 Villarini and Vecchi (2012) project that Atlantic TC frequency will increase in the first half
598 of the twenty-first century, while no significant change is projected over the entire century.
599 Their method uses only SST as the statistical predictor and does not explicitly account for
600 changes in humidity or wind shear. Downscaling six CMIP5 models under the RCP8.5
601 emissions scenario using the statistical-deterministic downscaling method of Emanuel et al.
602 (2008), Emanuel (2013) projects a consistent increase in Atlantic TC frequency and Cat 4-5
603 frequency over the twenty-first century [Atlantic basin results from Emanuel (2013) are
604 reported in supplemental material of Knutson et al. (2020)].

A recent study explores the responses of TCs to climate change using coupled GCMs with increasingly fine resolution. While the global TC frequency decreases substantially in the 50-km model, the 25-km HiFLOR (the same model but with different experimental designs) shows no significant change, and when model biases are corrected, HiFLOR shows a significant increase in TC frequency (Vecchi et al., 2019). Nevertheless, compared to previous studies, the increase of 22% in TC frequency for the North Atlantic basin in HiFLOR is exceptionally large, especially under the RCP 4.5 emission scenario. Although the difference in the climate conditions may have contributed to the difference in the storm projection in HiFLOR, the main reason may be that storm activity in HiFLOR is more sensitive to climate change effects, as the increase in storm frequency of 8.5% in KE08 and no significant change in PepC (+2.2%), given the same HiFLOR climate, are closer to the estimations in previous studies.

Multiple possible mechanisms have been discussed to explain the increment or reduction in TC frequency. Possible hypothesized mechanisms for the reduction in TC frequency include a slowing of the large-scale tropical circulation due to increasing static stability (Sugi et al. 2002; Held and Zhao 2011; Bengtsson et al. 2007) or increases in the saturation deficit between the surface and middle troposphere (Emanuel et al. 2008). On the other hand, possible mechanisms for increasing TC frequency include increases in potential intensity, and, in particular, increases in the area over which the PI is sufficiently large to sustain genesis, due to the reduction in the meridional temperature gradient and relative warming at the poleward boundaries of the historical zones of TC activity (Fedorov et al. 2018; Viale and Merlis 2017).

While the large-scale thermodynamic environment is no doubt an important factor modulating the rate of TC genesis, it is well known that real TCs often, and perhaps always,

develop from pre-existing disturbances of independent physical origin. Experiments with high-resolution GCMs (Li et al. 2010; Vecchi et al. 2019; Sugi et al. 2020; Hsieh et al. 2020; Vidale et al. 2021; Yamada et al. 2021) have been used to explore such pre-existing disturbances and relate their frequency to the frequency of TCs. When these disturbances meet certain requirements, they are labeled "seeds", and their frequency is often the dominant control on overall TC frequency compared to the probability of their transitioning to TCs. For example, in Hsieh et al. (2020), seeds are defined as disturbances detected by a tracking algorithm whose relative vorticity lies in the interval of $4x10^{-4}$ s^{-1} and 10^{-3} s^{-1}. Weaker perturbations are identified as cloud clusters. However, it should be noted that, due to the spatial scale of TC seeds and the role of atmospheric convection in them, their simulation and sensitivity in GCMs may show model dependence arising from the effective resolution of a model's dynamical core and the model's physical parameterizations (Zhao et al. 2012). Developed based on HiFLOR TCs at the genesis stage using regression-based techniques, PepC does not explicitly model TC seeds or their transition to TCs. KE08 use a seeding rate that varies only with the absolute vorticity near the equator, but their seeds are much weaker than the seeds defined by Hsieh et al. (2020) and the transition of the KE08 seeds to an intensity commensurate with the Hsieh et al (2020) seeds displays considerable climate sensitivity. Research on the evolution of weak disturbances into TCs is an increasingly active endeavor in tropical meteorology.

5. Conclusion

In this study, we investigated the responses of TCs to climate change by comparing projected TCs downscaled from a high-resolution global climate model using statistical and statistical-deterministic methods with those directly resolved in the climate model under the

historical and future projected climates. The HiFLOR model is used to produce the climate projections, which drive the two downscaling frameworks. HiFLOR is able to explicitly simulate TCs that are realistic in a number of respects, and these HiFLOR-generated TCs are used as a reference in the comparisons. Three 70-year HiFLOR experiments, which represent the climate during the period of 1986–2005, 2016–35, and 2081–2100 under the RCP4.5 scenario, were performed to explore the effects of climate change. The statistical-deterministic downscaling method, KE08, of Emanuel et al. (2008) and the statistical downscaling method, PepC, of Jing and Lin (2020), were used to generate large samples of synthetic TCs for the North Atlantic basin, given the environmental climate change conditions as obtained from the HiFLOR projections.

We find that HiFLOR and, to lesser extent, KE08 simulate significantly more Atlantic TCs by the end of the twenty-first century, although the increases are not significant in the mid-twenty-first century, while PepC shows no significant change in TC frequency over the century. All simulation methods project significant increases in the frequency of both major hurricanes and Category 5 hurricanes by the end of the twenty-first century. The fraction of RI storms is also projected to increase significantly, which is consistent with previous studies (e.g., Emanuel 2017, Bhatia et al. 2018). The projected significant increase of RI storms is also consistent with the physical understanding that the rate of intensification scales with the square of the potential intensity (Emanuel 2012). The increase in the fraction of the most intense storms leads to a shift to higher intensity values of the entire LMI distribution under the warmer climate, with HiFLOR responding the most to climate change and PepC the least. This difference in the extent of responses of HiFLOR, KE08, and PepC results in very different tails of the LMI distributions under the future climate although the tails for the three datasets are very similar under the control climate. Nevertheless, the overall increases in TC

677 frequency and especially intensity under the warmer climate do not carry over to landfalling
678 TCs in all of the simulations. The return levels of landfall intensity for the US coastline
679 remain nearly the same for future projected conditions as for the control condition. However,
680 minor changes exist at regional scales. HiFLOR projects that the northeastern U.S., which has
681 the lowest TC threat, may see a moderate growth of the TC threat as the climate gets warmer.
682 In contrast, in Mexico, the landfalling TC threat may even slightly decrease under a warmer
683 climate according to HiFLOR projections. These regional trends do not exist in KE08 or
684 PepC.

685 In this study, we examined the performance of a newly developed statistical downscaling
686 approach, PepC, to TC climate change studies, in comparison with dynamic (HiFLOR) and
687 statistical-deterministic downscaling methods (KE08). We compare findings in this study
688 with previous projections and point out that the large increment of TC frequency in HiFLOR
689 (+22%) under the RCP 4.5 emission scenario is barely seen in previous studies based on
690 CMIP3 and CMIP5 models. The moderate increase in KE08 (+8.5%) and the insignificant
691 change in PepC (+2.2%) are closer to previous projections, though those projections were
692 based in many cases on lower-resolution models than HiFLOR. The increase in the overall
693 fraction of Category 4-5 hurricanes projected by HiFLOR (+126%) is also much larger than
694 that projected by KE08 (+46%), PepC (+45%), and previous studies. As all three simulations
695 are based on the same climate projection, the results indicate that the storm activity in
696 HiFLOR is more sensitive to climate change effects. On the other hand, statistical
697 downscaling models may be less sensitive to climate change effects. More work is needed to
698 further investigate potentials and limitations in TC statistical downscaling methods; possible
699 future work includes a downscaling study for other state-of-the-art climate models, such as
700 CMIP6 climate models. This study focuses on the uncertainty in TC modeling; for future TC

projections and applications in decision making, the uncertainty in future climate projections of large-scale environmental conditions, e.g., based on analyzing a range of CMIP6 models under various emission scenarios, should also be considered.

Acknowledgments.

This work is supported by National Science Foundation (grants 1520683 and 1652448).

Data Availability Statement.

The generated synthetic storm datasets are deposited to the NSF DesignSafe-CI and can be accessed online (https://www.designsafe-ci.org/data/browser//xxx).

REFERENCES

Bengtsson, L., Hodges, K. I., Esch, M., Keenlyside, N., Kornblueh, L., Luo, J.-J., & Yamagata, T. (2007). How may tropical cyclones change in a warmer climate? Tellus A, 59(4), 539–561. http://doi.org/10.1111/j.1600-0870.2007.00251.x

Benjamini, Y. & Yekutieli, D. (2001) The control of the false discovery rate in multiple testing under dependency. The Annals of Statistics. 29(4), 1165-1188.

Benjamini, Y., & Yekutieli, D. (2005). False discovery rate adjusted multiple confidence intervals for selected parameters. Journal of the American Statistical Association, 100(469), 71?81. doi:10.1198/016214504000001907

Bhatia, K., Vecchi, G., Murakami, H., Underwood, S., & Kossin, J. (2018). Projected Response of Tropical Cyclone Intensity and Intensification in a Global Climate Model. Journal of Climate, 31(20), 8281–8303. http://doi.org/10.1175/JCLI-D-17-0898.1

724 Bhatia, K., G.A. Vecchi, T. Knutson, H. Murakami, J. Kossin, K. Dixon and C. Whitlock
725 (2019): An Increase in the Intensification Rates of Atlantic Hurricanes. Nature
726 Communications. doi: 10.1038/s41467-019-08471-z.

727 Bister, M., and K. A. Emanuel, 2002: Low frequency variability of tropical cyclone potential
728 intensity 1. Interannual to interdecadal variability. J. Geophys. Res.: Atmospheres, 107, 4801.

729 Camargo, S. J. (2013). Global and Regional Aspects of Tropical Cyclone Activity in the
730 CMIP5 Models. Dx.Doi.org, 26(24), 9880–9902. http://doi.org/10.1175/JCLI-D-12-00549.1

731 Davis, C. A., 2018: Resolving tropical cyclone intensity in models. Geophys. Res. Lett., 45,
732 2082–2087, https://doi.org/10.1002/2017GL076966.

733 DeMaria,M., and J. Kaplan, 1995: A simple empirical model for predicting the decay of
734 tropical cyclone winds after landfall. J. Appl. Meteor., 34, 2499–2512,
735 https://doi.org/10.1175/1520-0450(1995)034,2499:ASEMFP.2.0.CO;2

736 Emanuel, K., Ravela, S., Vivant, E. & Risi, C. A statistical deterministic approach to
737 hurricane risk assessment. Bull. Am. Meteorol. Soc. 87, 299–314 (2006).

738 Emanuel, K., R. Sundararajan, J. Williams, and J. Williams, 2008: Hurricanes and Global
739 Warming: Results from Downscaling IPCC AR4 Simulations. Bull. Amer. Meteor. Soc, 89,
740 347–368, doi:10.1175/BAMS-89-3-347.

741 Emanuel, K. (2010). Tropical Cyclone Activity Downscaled from NOAA-CIRES Reanalysis,
742 1908–1958. Journal of Advances in Modeling Earth Systems, 2(1), 1.
743 http://doi.org/10.3894/JAMES.2010.2.1

744 Emanuel, K., K. Oouchi, M. Satoh, T. Hirofumi, and Y. Yamada, 2010: Comparison of
745 explicitly simulated and downscaled tropical cyclone activity in a high-resolution global
746 climate model. J. Adv. Model. Earth Sys., 2, DOI:10.3894/JAMES.2010.2.9.

747 Emanuel, K., 2012: Self-stratification of tropical cyclone outflow: Part II: Implications for
748 storm intensification. *J. Atmos. Sci.*, **69**, 988-996. Corrigendum.

749 Emanuel, K. (2013). Downscaling CMIP5 climate models shows increased tropical cyclone
750 activity over the 21st century. Proceedings of the National Academy of Sciences, 110(30),
751 12219–12224. http://doi.org/10.1073/pnas.1301293110

752 Emanuel, K., 2017: Will global warming make hurricane forecasting more difficult? Bull.
753 Amer. Meteor. Soc., 98, 495-501.

754 Fedorov, A. V., L. Muir, W. R. Boos, and J. Studholme, 2018: Tropical cyclogenesis in warm
755 climates simulated by a cloud-system resolving model. Climate Dynamics, 52, 107–127.

756 Garner, A. J., and et al, 2017: Impact of climate change on New York City's coastal flood
757 hazard: Increasing flood heights from the preindustrial to 2300 CE. Proc. Natl. Acad. Sci.
758 USA, 114, 11 861–11 866, https://doi.org/10.1073/pnas.1703568114.

759 Harris, L. M., S.-J. Lin, and C. Tu, 2016: High-resolution climate simulations using GFDL
760 HiRAM with a stretched global grid. J. Climate, 29, 4293–4314, https://doi.org/10.1175/
761 JCLI-D-15-0389.1.

762 Hsieh, T.L., Vecchi, G.A., Yang, W., Held, I.M. and Garner, S.T., 2020. Large-scale control
763 on the frequency of tropical cyclones and seeds: a consistent relationship across a hierarchy
764 of global atmospheric models. Climate Dynamics, 55(11), pp.3177-3196.

765 Held, I. M., and M. Zhao, 2011: The response of tropical cyclone statistics to an increase in
766 CO2 with fixed sea surface temperatures. J. Climate, 24, 5353–5364.

767 Jing, R., & Lin, N. (2020). An environment-dependent probabilistic tropical cyclone model.
768 Journal of Advances in Modeling Earth Systems, 12, e2019MS001975.
769 https://doi.org/10.1029/2019MS001975

770 Knapp, K. R., M. C. Kruk, D. H. Levinson, H. J. Diamond, and C. J. Neumann, 2010: The
771 International Best Track Archive for Climate Stewardship (IBTrACS): Unifying tropical
772 cyclone data. Bull. Amer. Meteor. Soc., 91, 363–376, https://doi.org/
773 10.1175/2009BAMS2755.1.

774 Knutson, T. R., R. E. Tuleya, and Y. Kurihara, 1998: Simulated increase of hurricane
775 intensities in a CO2-warmed climate. Science, 279, 1018–1020,
776 https://doi.org/10.1126/science.279.5353.1018.

777 Knutson, T. R., and R. E. Tuleya, 2004: Impact of CO2-induced warming on simulated
778 hurricane intensity and precipitation: Sensitivity to the choice of climate model and
779 convective parameterization. J. Climate, 17, 3477–3495, https://doi.org/ 10.1175/1520-
780 0442(2004)017,3477:IOCWOS.2.0.CO;2.

781 Knutson, T.R., Sirutis, J.J., Garner, S.T., Vecchi, G.A. and Held, I.M., 2008. Simulated
782 reduction in Atlantic hurricane frequency under twenty-first-century warming
783 conditions. Nature Geoscience, 1(6), pp.359-364.

784 Knutson, T. R. and Coauthors, 2013: Dynamical downscaling projections of twenty-first-
785 century Atlantic hurricane activity: CMIP3 and CMIP5 model-based scenario. J. Climate, 26,
786 6591–6617, doi:10.1175/JCLI-D-12-00539.1.

787 Knutson, T. R., J. J. Sirutis, M. Zhao, R. E. Tuleya, M. Bender, G. A. Vecchi, G. Villarini,
788 and D. Chavas, 2015: Global projections of intense tropical cyclone activity for the late
789 twenty-first century from dynamical downscaling of CMIP5/RCP4.5 scenarios. J. Climate,
790 28, 7203–7224, https://doi.org/10.1175/JCLI-D-15-0129.1.

791 Knutson, T., Camargo, S. J., Chan, J. C. L., Emanuel, K., Ho, C.-H., Kossin, J., et al. (2020).
792 Tropical Cyclones and Climate Change Assessment: Part II: Projected Response to

793 Anthropogenic Warming. Bulletin of the American Meteorological Society, 101(3), E303–
794 E322. http://doi.org/10.1175/BAMS-D-18-0194.1

795 Korty, R. L., K. A. Emanuel, M. Huber, and R. A. Zamora, 2017: Tropical cyclones
796 downscaled from simulations with very high carbon dioxide levels. J. Climate, 30, 649–667,
797 https://doi.org/10.1175/JCLI-D-16-0256.1

798 Kossin, J. P., T. L. Olander, and K. R. Knapp, 2013: Trend analysis with a new global record
799 of tropical cyclone intensity. J. Climate, 26, 9960–9976, https://doi.org/10.1175/JCLI-D-13-
800 00262.1.

801 Lee, C.-Y., Tippett, M. K., Camargo, S. J., & Sobel, A. H. (2015). Probabilistic multiple
802 linear regression modeling for tropical cyclone intensity. Monthly Weather Review, 143,
803 933–954.

804 Lee, C.-Y., Tippett, M. K., Sobel, A. H., & Camargo, S. J. (2016). Autoregressive modeling
805 for tropical cyclone intensity climatology. Journal of Climate, 29, 7815–7830.

806 Lee, C.-Y., M. K. Tippett, A. H. Sobel, and S. J. Camargo, 2018: An environmentally forced
807 tropical cyclone hazard model. J. Adv. Model. Earth Syst., 10, 223–241.

808 Lee, C.-Y., Camargo, S. J., Sobel, A. H., & Tippett, M. K. (2020). Statistical-dynamical
809 downscaling projections of tropical cyclone activity in a warming climate: Two diverging
810 genesis scenarios. Journal of Climate, JCLI–D–19–0452.1. http://doi.org/10.1175/JCLI-D-19-
811 0452.1

812 Li T, Min HK, Ming Z, Jong-Seong K, Jing-Jia L, Weidong Y (2010) Global warming shifts
813 Pacific tropical cyclone location. Geophys Res Lett. https://doi.org/10.1029/2010GL045124

814 Liu, Maofeng, Gabriel A Vecchi, J A Smith, and Thomas R Knutson, (2019). Causes of large
815 projected increases in hurricane precipitation rates with global warming. npj Climate and
816 Atmospheric Science, *2*, 38, DOI:10.1038/s41612-019-0095-3

817 Manganello, J.V., Hodges, K.I., Dirmeyer, B., Kinter III, J.L., Cash, B.A., Marx, L., Jung, T.,
818 Achuthavarier, D., Adams, J.M., Altshuler, E.L. and Huang, B., 2014. Future changes in the
819 western North Pacific tropical cyclone activity projected by a multidecadal simulation with a
820 16-km global atmospheric GCM. Journal of Climate, 27(20), pp.7622-7646.

821 Marsooli, R., Lin, N., Emanuel, K., & Feng, K. (2019). Climate change exacerbates hurricane
822 flood hazards along US Atlantic and gulf coasts in spatially varying patterns. Nature
823 Communications, 10(1), 1–9. https://doi.org/10.1038/s41467-019-11755-z

824 Mendelsohn, R., Emanuel, K., Chonabayashi, S., & Bakkensen, L. (2012). The impact of
825 climate change on global tropical cyclone damage. Nature Climate Change, 2(3), 205–209.
826 https://doi.org/10.1038/nclimate1357

827 Murakami, H., and Coauthors, 2012: Future changes in tropical cyclone activity projected by
828 the new high-resolution MRI-AGCM. J. Climate, 25, 3237–3260,
829 https://doi.org/10.1175/JCLI-D-11-00415.1.

830 Murakami, H., Anderson, W. G., Gudgel, R. G., Lin, S.-J., Zeng, F., Vecchi, G. A., et al.
831 (2015). Simulation and Prediction of Category 4 and 5 Hurricanes in the High-Resolution
832 GFDL HiFLOR Coupled Climate Model*. Dx.Doi.org, 28(23), 9058–9079.
833 http://doi.org/10.1175/JCLI-D-15-0216.1

834 Murakami, H., G. A. Vecchi, G. Villarini, T. L. Delworth, R. Gudgel, S. Underwood, X.
835 Yang, W. Zhang, and S. -J Lin. (2016): "Seasonal Forecasts of Major Hurricanes and

836 Landfalling Tropical Cyclones using a High-Resolution GFDL Coupled Climate Model."
837 Journal of Climate 29 (22): 7977-7989. doi:10.1175/JCLI-D-16-0233.1.

838 Rayner, N. A., D. E. Parker, E. B. Horton, C. K. Folland, L. V. Alexander, D. P. Rowell, E.
839 C. Kent, and A. Kaplan, 2003: Global analyses of sea surface temperature, sea ice, and night
840 marine air temperature since the late nineteenth century. J. Geophys. Res., 108, 4407,
841 https://doi.org/10.1029/2002JD002670.

842 Schade, L. R., and K. A. Emanuel, 1999: The ocean's effect on the intensity of tropical
843 cyclones: Results from a simple coupled atmosphere–ocean model. J. Atmos. Sci., 56, 642–
844 651, https://doi.org/10.1175/1520-0469(1999)056<0642:TOSEOT>2.0.CO;2

845 Scoccimarro, E., S. Gualdi, G. Villarini, G. A. Vecchi, M. Zhao, K. Walsh, and A. Navarra,
846 2014: Intense precipitation events associated with landfalling tropical cyclones in response to
847 a warmer climate and increased co2. Journal of climate, 27 (12), 4642–4654.

848 Scoccimarro, E., Fogli, P.G., Reed, K.A., Gualdi, S., Masina, S. and Navarra, A., 2017.
849 Tropical cyclone interaction with the ocean: The role of high-frequency (subdaily) coupled
850 processes. Journal of Climate, 30(1), pp.145-162.

851 Small, R. J., Bacmeister, J., Bailey, D., Baker, A., Bishop, S., Bryan, F., ... & Jochum, M.
852 (2014). A new synoptic scale resolving global climate simulation using the Community Earth
853 System Model. Journal of Advances in Modeling Earth Systems, 6(4), 1065-1094.

854 Stansfield, A. M., Reed, K. A., & Zarzycki, C. M. (2020). Changes in Precipitation From
855 North Atlantic Tropical Cyclones Under RCP Scenarios in the Variable-Resolution
856 Community Atmosphere Model. Geophysical Research Letters, 47(12), e2019GL086930.

857 Sugi, M., A. Noda, and N. Sato, 2002: Influence of the global warming on tropical cyclone
858 climatology: An experiment with the JMA global climate model. Meteor. Soc. Japan, 80,
859 249-272.

860 Sugi, M., Y. Yamada, K. Yoshida, R. Mizuta, M. Nakano, C. Kodama, and M. Satoh,2020:
861 Future changes in the global frequency of tropical cyclone seeds. SOLA,16, 70–
862 74,doi:10.2151/sola.2020-012

863 Tory, K. J., S. S. Chand, J. L. McBride, H. Ye, and R. A. Dare, 2013: Projected changes in
864 late-twenty-first-century tropical cyclone frequency in 13 coupled climate models from phase
865 5 of the Coupled Model Intercomparison Project. J. Climate, 26, 9946– 9959,
866 https://doi:10.1175/JCLI-D-13-00010.1.

867 van der Wiel, K., S. B. Kapnick, and G. A. Vecchi, 2017: Shifting patterns of mild weather in
868 response to projected radiative forcing. Climatic Change, 140, 649–658, https://doi.org/
869 10.1007/s10584-016-1885-9.

870 Van Vuuren, D. P., and Coauthors, 2011: The representative concentration pathways: An
871 overview. Climatic Change, 109, 5–31, https://doi.org/10.1007/s10584-011-0148-z.

872 Viale, F., and T. M. Merlis, 2017: Variations in tropical cyclone frequency response to solar
873 and CO2 forcing in aquaplanet simulations. J. Adv. Model Earth Syst., 9, 4–18.

874 Vidale, P.L., Hodges, K., Vannière, B., Davini, P., Roberts, M.J., Strommen, K., Weisheimer,
875 A., Plesca, E. and Corti, S., 2021. Impact of stochastic physics and model resolution on the
876 simulation of tropical cyclones in climate GCMs. Journal of Climate, 34(11), pp.4315-4341.

877 Vecchi, G. A., and Coauthors, 2014: On the seasonal forecasting of regional tropical cyclone
878 activity. J. Climate, 27, 7994–8016, https://doi.org/10.1175/JCLI-D-14-00158.1.

879 Vecchi, G. A., and Coauthors, 2019. Tropical cyclone sensitivities to CO2 doubling: roles of
880 atmospheric resolution, synoptic variability and background climate changes. Climate
881 Dynamics. doi: 10.1007/s00382-019-04913-y

882 Vickery, P. J., Skerlj, P. F., & Twisdale, L. A. (2000). Simulation of hurricane risk in the
883 U.S. using empirical track model. Journal of Structural Engineering, 126(10), 1222–1237.
884 https://doi.org/10.1061/(ASCE)0733-9445(2000)126:10(1222)

885 Villarini, G., Vecchi, G. Twenty-first-century projections of North Atlantic tropical storms
886 from CMIP5 models. Nature Clim Change 2, 604–607 (2012).
887 https://doi.org/10.1038/nclimate1530

888 Walsh, K. J., and Coauthors, 2016: Tropical cyclones and climate change. Wiley
889 Interdisciplinary Reviews: Climate Change, 7, 65–89.

890 Wehner, Michael F., et al. "The effect of horizontal resolution on simulation quality in the C
891 ommunity a tmospheric M odel, CAM 5.1." Journal of Advances in Modeling Earth Systems
892 6.4 (2014): 980-997.

893 Wilks, D. S., 2011: Statistical Methods in the Atmospheric Sciences. 3rd ed. International
894 Geophysics Series, Vol. 100, Academic Press, 676 pp.

895 Yamada, Y., Kodama, C., Satoh, M., Sugi, M., Roberts, M.J., Mizuta, R., Noda, A.T.,
896 Nasuno, T., Nakano, M. and Vidale, P.L., 2021. Evaluation of the contribution of tropical
897 cyclone seeds to changes in tropical cyclone frequency due to global warming in high-
898 resolution multi-model ensemble simulations. Progress in Earth and Planetary Science, 8(1),
899 pp.1-17.

900 Yamada, Y., and Coauthors, 2020: Evaluation of the contribution of tropical cyclone seeds to
901 changes in tropical cyclone frequency due to global warming in high-resolution multi-model

902 ensemble simulations. Progress in Earth and Planetary Science, doi:10.21203/rs.3-20670/v1,
903 in review

904 Zhang, W., and Coauthors, 2016: Improved simulation of tropical cyclone responses to
905 ENSO in the western North Pacific in the high-resolution GFDL HiFLOR coupled climate
906 model. J. Climate, 29, 1391–1415, https://doi.org/10.1175/ JCLI-D-15-0475.1.

907 Zhao, Ming, Isaac M Held, and Shian-Jiann Lin, 2012: Some counter-intuitive dependencies
908 of tropical cyclone frequency on parameters in a GCM. Journal of the Atmospheric Sciences,
909 69(7), DOI:10.1175/JAS-D-11-0238.1.

910

911

912 TABLES

	Total Storms		**Major Hurricanes**		**Category 4**		**Category 5**		**RI Storms**	
	Early	Late	Early	Late	Early	Late	Early	Late	Early	Late
HiFLOR	+8.2%	**+22.4%**	**+24.0%**	**+60.4%**	+30.4%	**+103.2%**	**+60.0%**	**+540.0%**	**+39.6%**	**+76.0%**
KE08	-4.4%	**+8.5%**	+2.2%	**+37.8%**	-21.1%	+13.3%	+108.3%	**+250.0%**	-11.2%	**+20.5%**
PepC	-0.6%	+2.2%	+2.3%	**+17.1%**	+4.2%	**+29.4%**	**+1.1%**	**+53.6%**	+1.8%	**+10.8%**

913

914 Table 1. The percent difference of the number of total storms, major hurricanes, Category 4
915 hurricanes, Category 5 hurricanes, and number of storms that undergo RI in HiFLOR, KE08,
916 and PepC, between the HiFLOR climate change simulations and the HiFLOR control
917 simulation. For each storm type, the first entry in the table cell is the percent difference
918 between the 2016–35 and 1986–2005 simulations, and the second entry is the percent

difference between the 2081–2100 and 1986–2005 simulations. Positive values indicate percent increases in the climate change simulation. Statistically significant changes are bolded.

FIGURES

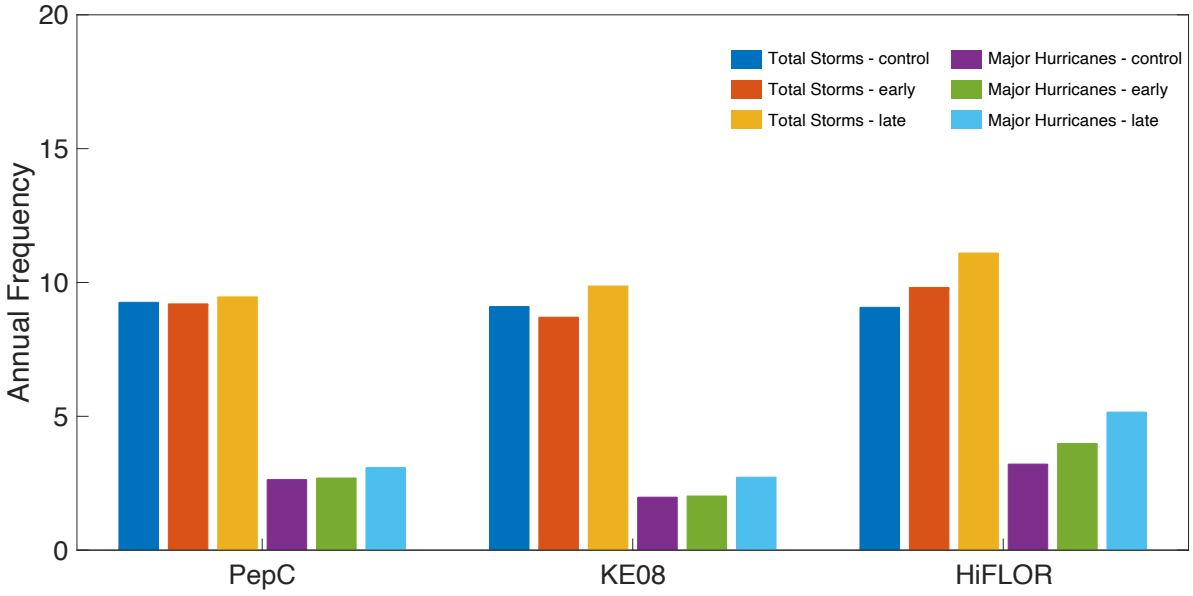

Fig. 1 Annual frequency of total storms and major hurricanes (wind speed >95kt) for HiFLOR, KE08, and PepC in the control (1986–2005) and climate change (2016–35, "early" and 2081–2100, "late") experiments.

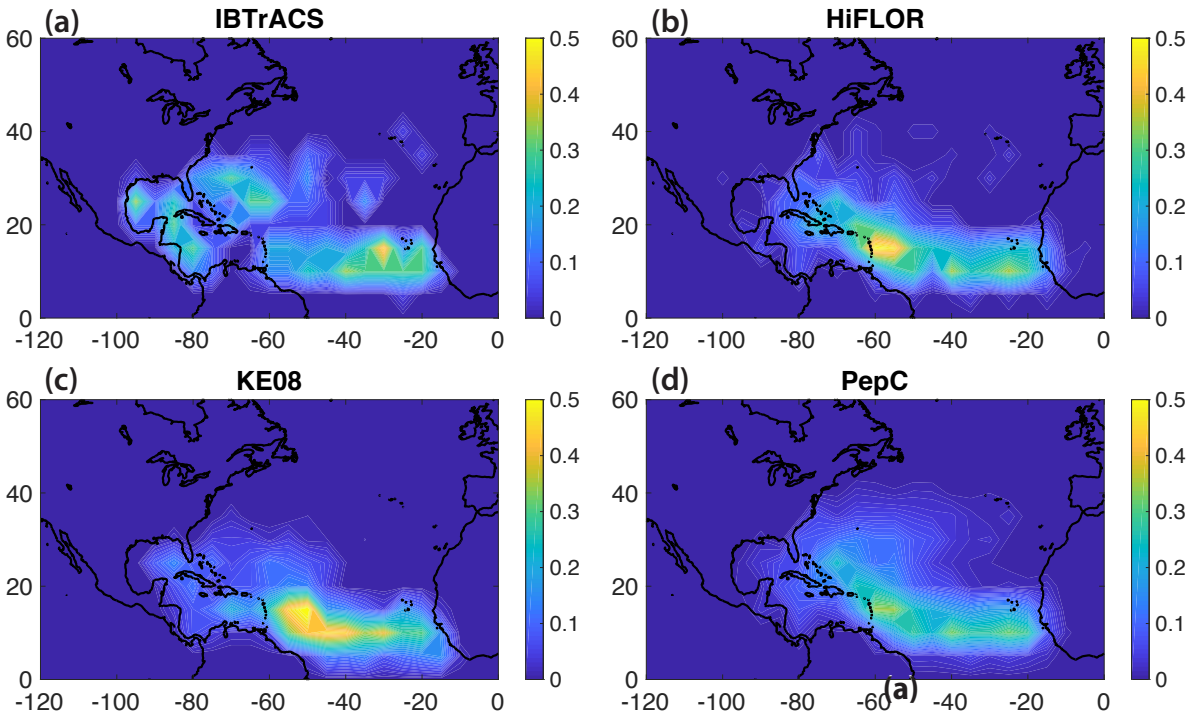

Fig. 2 Comparison of the spatial distribution of genesis in (a) IBTrACS, (b) HiFLOR, (c) KE08 and (d) PepC in the control experiment. Color indicates the number per year of storms in each 5°×5° grid box (after calibration) smoothed with a Gaussian lowpass filter.

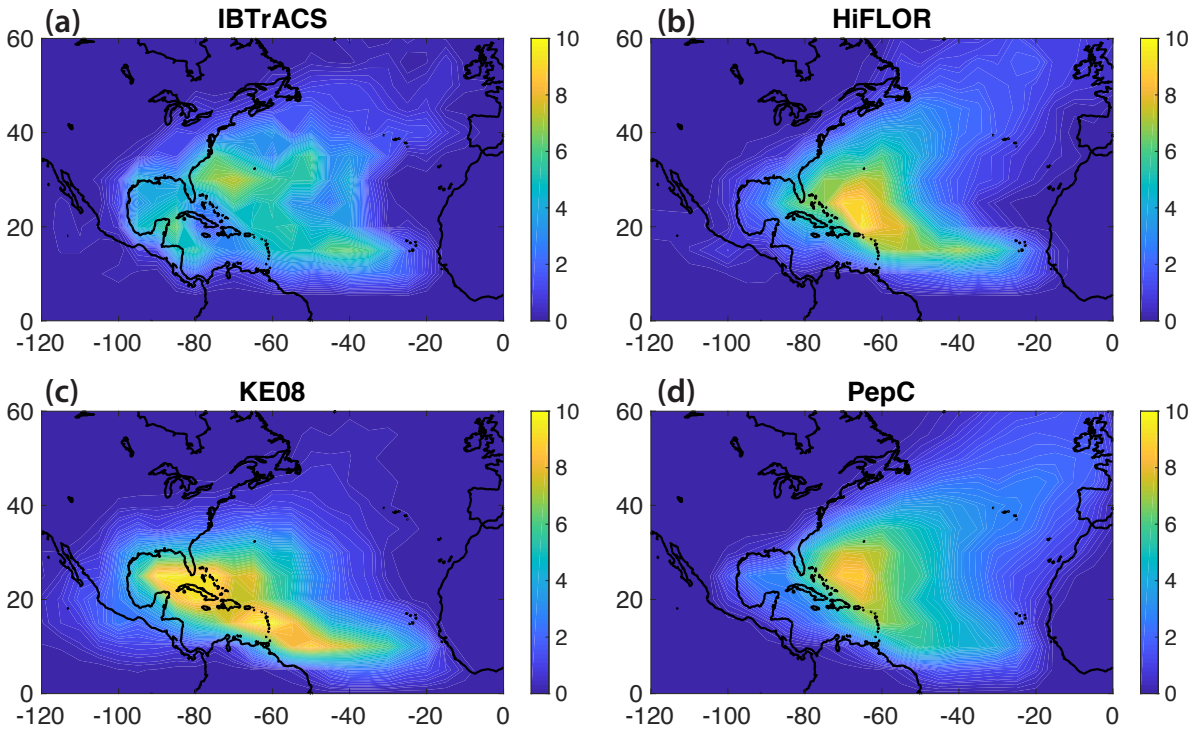

Fig. 3 Comparison of track density in (a) IBTrACS, (b) HiFLOR, (c) KE08, and (d) PepC under the control experiment. Track density is calculated as the number of times per year TC tracks pass into each 5°×5° grid box smoothed with a Gaussian lowpass filter.

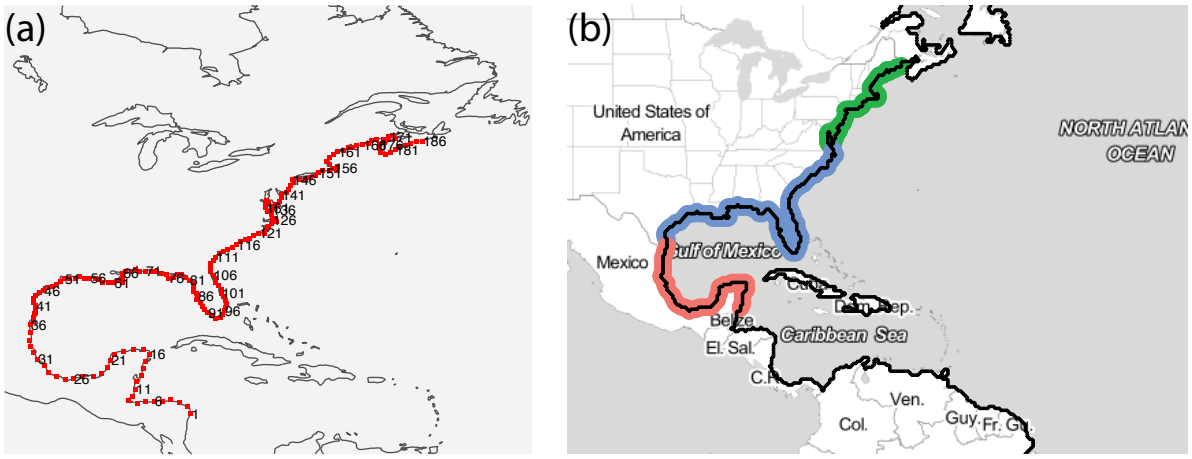

Fig. 4 Illustrations of locations and areas along the North Atlantic coastline considered in this study: (a) locations of considered mileposts along Mexico (every 100 km) and U.S. (every 50 km) coastline; (b) locations of four regions: North Atlantic coastline (green, blue, and red segments shown on the map, all 186 MPs), Northeastern U.S. from Maine to Virginia (green segment, MP 128-186), Southeastern U.S. from North Carolina to Florida plus Gulf Coast of the U.S. (blue segment, MP 41-128) and Gulf Coast of Mexico (red segment, MP 1-40).

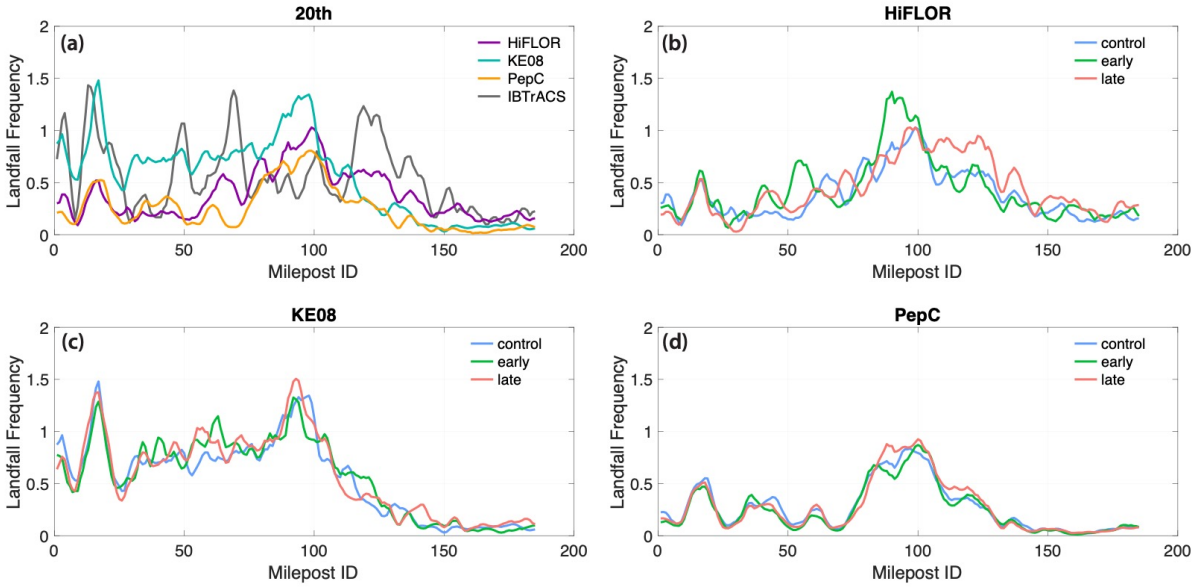

975

976 Fig. 5 Comparison of annual landfall frequency at each of the 186 mileposts (as shown in
977 Fig. 4) along the North Atlantic coastline (a) under the control experiment and (b-d) for each
978 dataset under the warming climate.

979

980

981

982

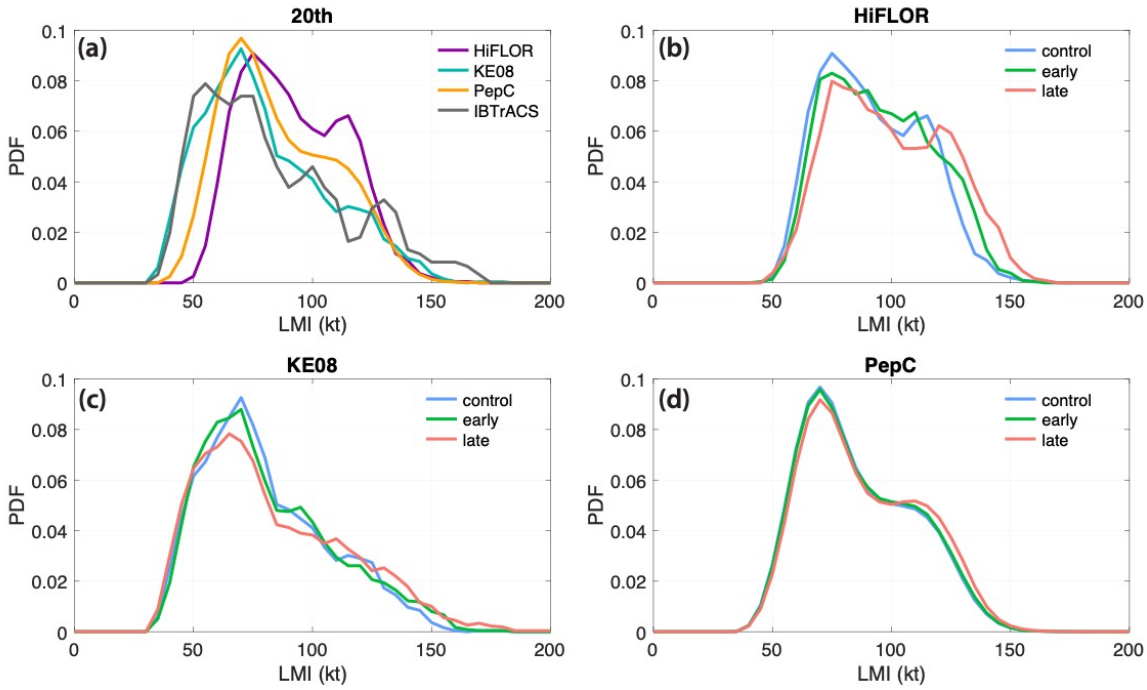

983

984 Fig. 6 Comparison of probability density function (PDF) of lifetime maximum intensity
985 (LMI) in (a) the control experiment and (b-d) for each dataset under the warming climate.
986 Raw data are grouped in 5-kt bins and smoothed by a moving average window with width of
987 15 kts.

988

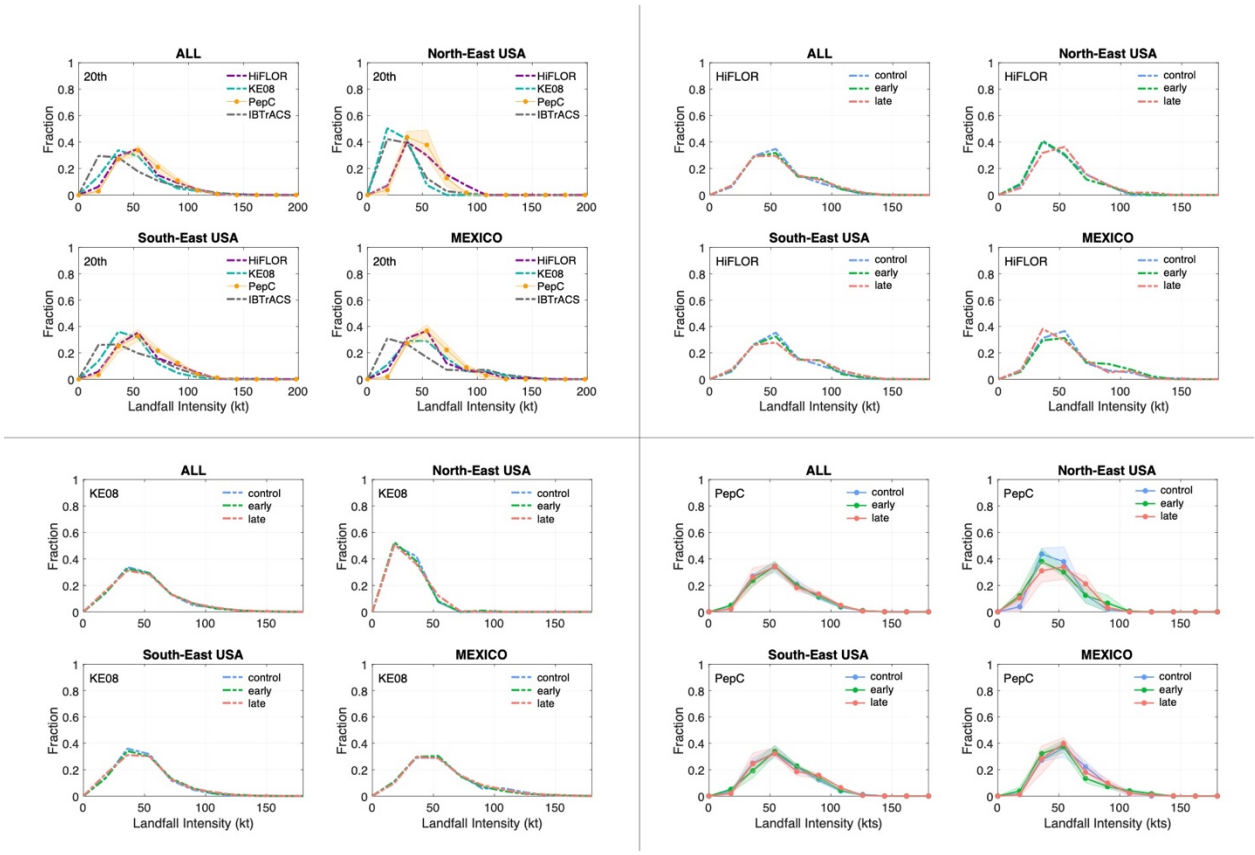

989

990

991 Fig. 7 Probability density function (PDF) of TC landfall intensity in the control, "early",
992 and "late" experiments. The four sub-figures on top left are comparisons of historical records
993 (IBTrACS) with HiFLOR, KE08, PepC in the control experiment. Other sub-figures show
994 climate effects on landfall intensity for HiFLOR, KE08, and PepC. Four regions defined in
995 Fig. 4 are examined. In PepC, the shadings show 25th – 75th percentile uncertainty bounds
996 estimated from 100 realizations. TC landfall is defined as crossing the coastline for each
997 region.

998

999

1000

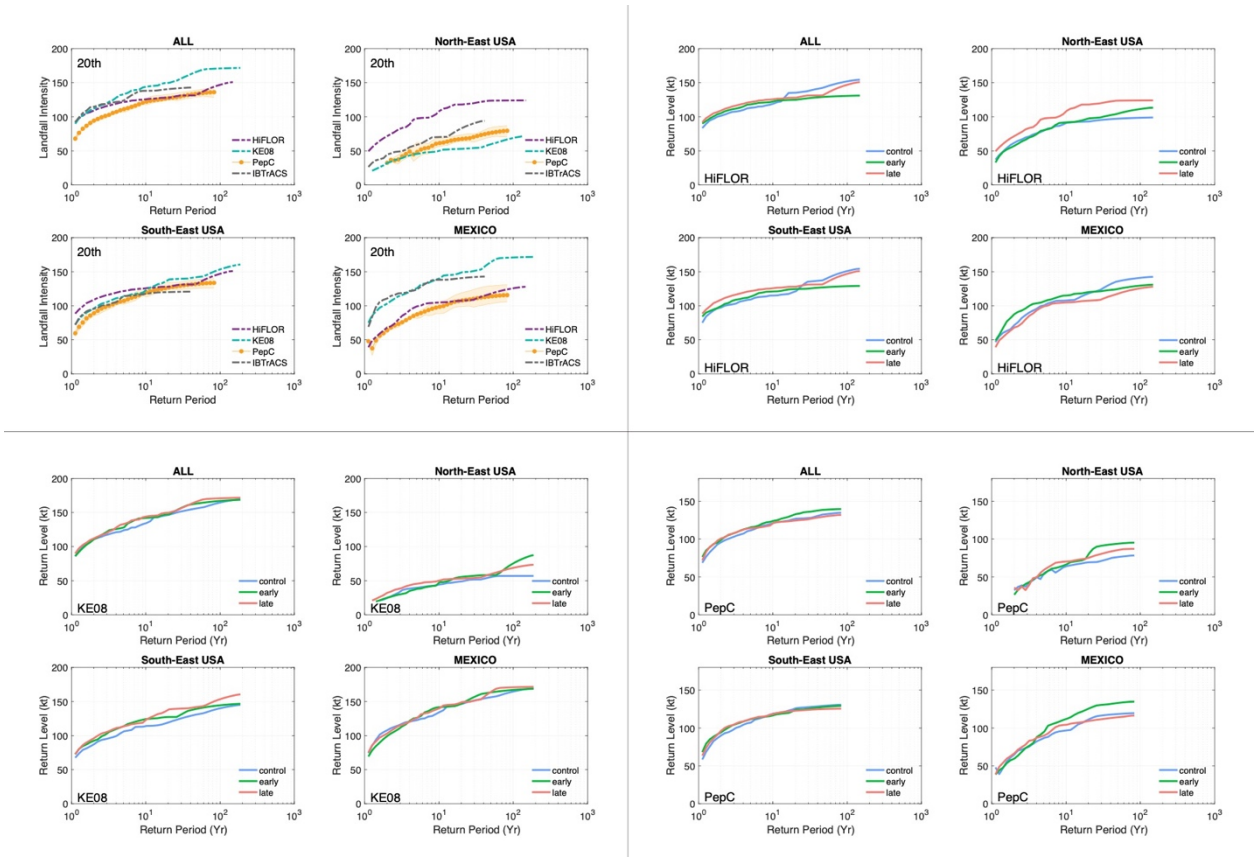

Fig. 8 Same as Fig. 7, but for the return period of TC landfall intensity.